Turkish Journal of Electrical Engineering & Computer Sciences

http://journals.tubitak.gov.tr/elektrik/

Research Article

Turk J Elec Eng & Comp Sci
(2017) 25: 3811 – 3826

doi:10.3906/elk-1606-410

Median filtering detection based on variations and residuals in image forensics

Kang Hyeon RHEE*
Department of Electronics Engineering, School of Design and Creative Engineering, Chosun University, Gwangju, Korea

Received: 25.06.2016 • **Accepted/Published Online:** 14.03.2017 • **Final Version:** 05.10.2017

Abstract: To attain a robust feature vector for median filtering detection (MFD) in digital forgery images, this paper presents a short feature vector that is made up of three types of feature sets. The first set is defined by the variation to be the 3-D length in the gradient difference of the intensity values of the adjacent row and column line pairs in the image, respectively. The second set is defined by the variation in the coefficient difference of the Fourier transform to be the 3-D length in the adjacent line pairs. The last set is defined by the residual image between an image and its reconstructed image by the gradient based on solving Poisson's equation, which is also the 3-D length. Two of the sets are extracted in the spatial and spectral domains of an image, respectively, and the last set is extracted from the residual image. The totally formed 9-D feature vector is subsequently trained in the support vector machine classifier for MFD. In the experimental results of the proposed variation- and residual-based MFD scheme, the area under the curve is achieved closer to 1. Despite a short feature vector, the evaluation of the proposed MFD scheme is graded as "Excellent (A)". In particular, the scheme detected good median filtering from the JPEG post-compression image for the cut-and-paste forgery image.

Key words: Coefficient of variation, digital image forgery, feature vector, Fourier transform, intensity gradient, median filtering forensics

1. Introduction

In image manipulations, a forger attempts to content-tamper the image, particularly preferring median filtering (MF) because it has the characteristics of nonlinear filtering based on order statistics. Therefore, MF detection is especially required for several altered images. The MF detector has become a significant forensic tool [1,2].

For the extraction of the feature vector, Kang et al. [3] obtained autoregressive (AR) coefficients as feature vectors via an AR model to analyze the median filter residual (MFR), which is the difference image between the values of the original image and its median-filtered image.

Typical MF detection schemes are the global and local feature set (GLF) [4], median filtering forensics (MFF) [1], the subtractive pixel adjacency matrix [5], the high-order local ternary pattern [6], MF detection by histogram features [7], the three type features of the MFR [8], and the MFR AR [3]. The remarkably employed occurrence of the block-center gray level (OBC) is partly combined in the MFF. The feature vector is short, but the classification result is quite accurate. MFF and GLF employ five entries; hence, the computing time to extract the feature vector using the various combined entries is long. The MFR AR has a short 10-D feature vector, and other schemes have a more extended feature vector to increase the classification ratio of

*Correspondence: khrhee@chosun.ac.kr

MF detected. After all, the feature vector for MF detection must be extracted with a shorter length and yet have the diversified characteristics of an image. Therefore, an MF detector meeting these requirements could be developed.

In this paper, a new variation- and residual-based MF detection scheme is proposed. The feature vector in the proposed scheme is constructed using the variations between the adjacent line pairs of row and column pixel values in an image, and the residual image is reconstructed using the gradient based on solving Poisson's equation (called RRP in this paper). The feature vector is composed of a three-part set: the first one is extracted from the spatial domain, the second one is extracted from the spectral domain in the image, and the last one is extracted from the RRP.

The rest of the paper is organized as follows: Section 2 briefly presents the specifications of the existing state-of-the-art MF detectors and the theoretical background of the MFR AR and MFF OBC schemes. In Section 3, a new feature vector from the variations and the residual in an image is computed for the MF detection. The construction of a feature vector is described. The experimental results of the proposed scheme are shown in Section 4, where the performance of the proposed scheme is compared with that of the MFR AR and MFF OBC. Finally, conclusions are drawn, and possible direction for future work is presented in Section 5.

2. Related background and works

Kang et al. proposed an MFR AR [3] using a 10-D feature vector that computed the AR coefficients of the difference image between the original image and its median-filtered image. The authors contrived to extract the feature vector from an image's MFR. The MFR is used in the AR model and is mathematically defined in [3] as:

$$d\left(i,j\right)=med_{w}\left(y\left(i,j\right)\right)-y\left(i,j\right), \tag{1}$$

where d is MFR, (i,j) is a pixel coordinate, and w is the MF window size. The AR coefficients are subsequently computed as:

$$a_{k}^{(r)}=AR\left(d^{(r)}\right), \tag{2}$$

$$a_{k}^{(c)}=AR\left(d^{(c)}\right), \tag{3}$$

$$a_{k}=\frac{a_{k}^{(r)}+a_{k}^{(c)}}{2}, \tag{4}$$

where r and c represent the row and column directions, respectively. k is the AR order number: $1\leq k\leq p$, where p is the maximum order number. Again, the AR coefficients are to be the difference image with the following:

$$d\left(i,j\right)=-\sum_{q=1}^{p}a_{k}^{(r)}d\left(i,j-q\right)+\varepsilon^{(r)}(i,j), \tag{5}$$

$$d\left(i,j\right)=-\sum_{q=1}^{p}a_{k}^{(c)}d\left(i-q,j\right)+\varepsilon^{(c)}(i,j), \tag{6}$$

where $\varepsilon^{(r)}(i,j)$ and $\varepsilon^{(c)}(i,j)$ are the prediction errors [9], and p is a surrounding range of (i,j).

Yuan [1] proposed detecting MF by measuring the relationships among the pixels within a 3 × 3 window in an image. That includes features such as the distribution of the block median pixel value and the distribution of the number of distinct gray levels within a window. Different entries of MFF are then heuristically combined to produce a new index. A binary decision uses the index to determine whether the image has undergone MF. In a median-filtered image, the author believes that the gray level of the block center should occur more frequently in the block after MF. The feature set of the OBC [1] is defined as:

$$\mathbf{h}^{OBC} = (h_1^{OBC}, h_2^{OBC}, \ldots, h_{s^2}^{OBC}), \tag{7}$$

where $h_i^{OBC} = \frac{\sum_{k=1}^{|\varepsilon|} \delta(|\{j|y_j^k = y_m^k\}|, i)}{|\varepsilon|}$, $j \in \{1, 2, \ldots, s^2\}$. The subscript here denotes the number of times that the block-center gray level occurs in a block.

3. Proposed MF detection scheme

In this section, the proposed new feature vector in this study is introduced. The proposed scheme considers the feature vector with a short length and high performance and employs the gradient nature in the spatial and spectral domain of the image. The extracted feature vector is composed of three subsets and will also serve as a basis for a single scalar discriminating feature. Three sets of discriminating features from the variation between the adjacent line pairs and the reconstructed image residual are computed. The formation procedure of these features is described in this section.

3.1. Gradient of adjacent line pairs

3.1.1. Variation in the spatial domain

In an image x, the intensity gradients between the adjacent line pairs (the row r and column c directions) are defined as $\mathrm{G}^{(r)}$ and $\mathrm{G}^{(c)}$, respectively [2], as follows:

$$G^{(r)}(i,j) = 2 \cdot x(i,j) - x(i-1,j) - x(i+1,j), \tag{8}$$

$$G^{(c)}(i,j) = 2 \cdot x(i,j) - x(i,j-1) - x(i,j+1). \tag{9}$$

The variations in $\mathrm{G}^{(r)}$ and $\mathrm{G}^{(c)}$ are defined as $\mathrm{VG}^{(r)}$ and $\mathrm{VG}^{(c)}$, respectively, and then VG_k is derived as follows:

$$VG_k = (VG_k^{(r)} + VG_k^{(c)})/2, \tag{10}$$

where k is the dimensional length.

3.1.2. Variation in the spectral domain

Furthermore, the coefficient (FT_{coeff}) gradients of the Fourier transform between the adjacent line pairs are defined as $\mathrm{GF}^{(r)}$ and $\mathrm{GF}^{(c)}$, respectively [2], as follows:

$$GF^{(r)}(i,j) = 2 \cdot FT_{coeff}(x(i,j)) - FT_{coeff}(x(i-1,j)) - FT_{coeff}(x(i+1,j)), \tag{11}$$

$$GF^{(c)}(i,j) = 2 \cdot FT_{coeff}(x(i,j)) - FT_{coeff}(x(i,j-1)) - FT_{coeff}(x(ij+1)). \tag{12}$$

The variations in $\mathrm{GF}^{(r)}$ and $\mathrm{GF}^{(c)}$ are defined as $\mathrm{VF}^{(r)}$ and $\mathrm{VF}^{(c)}$, respectively, and then VF_k is derived as follows:

$$VF_k = (VF_k^{(r)} + VF_k^{(c)})/2. \tag{13}$$

3.1.3. Reconstructing the image residual using the gradient based on solving Poisson's equation

The sum of the differentiation of gradients $\mathrm{G}^{(r)}$ and $\mathrm{G}^{(c)}$ yields a Laplacian image, which is the boundary image f [10]. The boundary point of f is defined as f_{bp}:

$$f_{bp}(r,c) = f(r,c+1) + f(r,c-1) + f(r-1,c) + f(r+1,c) - 4f(r,c). \tag{14}$$

It contains image intensity at the boundaries as follows:

$$\nabla^2 f = G_c^{(r)} + G_r^{(c)} - 4f(r,c). \tag{15}$$

The contribution of f_{bp} is defined as f_c:

$$f_c = f - f_{bp}. \tag{16}$$

With the gradient based on solving Poisson's equation using discrete sine transform (DST), a *sin* component of $f_c$is defined as f_c_sin:

$$f_c\_sin = DST(f_c). \tag{17}$$

The f_{ev} (the set of eigenvalues of f_c_sin) is subsequently computed, followed by the reconstructed image z [11] by inverse discrete sine transform (IDST) as follows:

$$z = IDST(f_{ev}). \tag{18}$$

The difference between the original x and the reconstructed image z is used to extract the feature set. The difference refers to the RRP, which is mathematically defined as:

$$RRP = |z - x|. \tag{19}$$

In Figure 1, an original image, the reconstructed image resulting from solving Poisson's equation, and the RRP image are shown, respectively.

Figure 1. Residual image by the gradient based on solving Poisson's equation: a) original image; b) reconstructed image by solving Poisson's equation; c) RRP image.

3.2. Feature vector structure of the variation- and residual-based MF detector

For the proposed variation- and residual-based MF detection scheme, the feature vector is constructed in the flow diagram shown in Figure 2. In the spatial domain part of the figure, the variations of the gradient differences between the adjacent lines in an image are computed by Eq. (10); in the spectral domain part, the variation of FT_{coeff} differences in an image is computed by Eq. (13). In the residual part, the RRP image is obtained with Eq. (19).

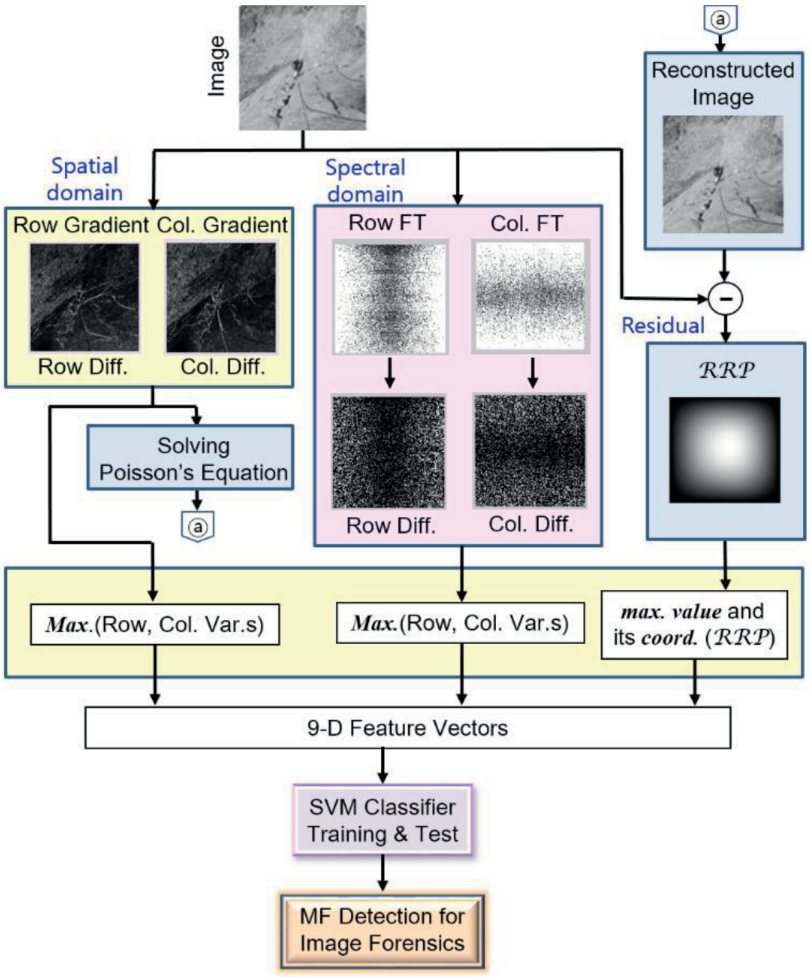

Figure 2. Flow diagram of the proposed variation- and residual-based MF detection algorithm.

In Figure 3, the constructed 9-D feature vector for the proposed MF detector is shown. The first set [1:3] is related to the variation, which represents the differences in the intensity values of the adjacent line pairs. This is computed in the spatial domain. The second set [4:6] is related to the variation represented by the differences between the FT coefficient values of the adjacent line pairs. This is computed in the spectral domain. The third set [7:9] is related to the residual image between an original image and its reconstructed image obtained by the gradient-based solving of Poisson's equation.

In the first and second feature sets, the k range is three, which are the three maximum values of both VG_k and VF_k, respectively. The third feature set consists of the maximum value and its coordinates i and j in the RRP image, respectively.

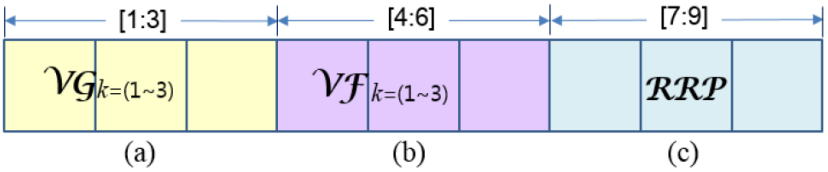

Figure 3. The feature vector for the variation- and residual-based MF detection proposed: a) differences in the intensity gradients VG between adjacent line pairs; b) differences in Fourier transform coefficients VF between adjacent line pairs; c) maximum value and its coordinates i and j of the RRP image.

The proposed complete MF detection scheme is shown in Algorithm 1.

Algorithm 1: Proposed median filtering detection Approach

Input:

- Query image $\boldsymbol{x}(i,j)$
- Block window size $\boldsymbol{w}$

Output:

- Area under ROC curve ***AUC***
- Classification ratio $\boldsymbol{\delta}$
- Minimal average decision error $\boldsymbol{P_e}$
- True positive and false positive rates $\underline{\boldsymbol{P}_{\mathrm{TP}}@P_{\mathrm{FP}}=0.01}$
- Median filtering detection ***MFD***

Feature extraction:

1: $\mathcal{VG}$ ← max. 3 gradient values of adjacent line pairs($\boldsymbol{x}(i,j)$)

2: $\mathcal{VF}$ ← max. 3 coefficient values of Fourier transform($\boldsymbol{x}(i,j)$)

3: $\mathcal{RRP}$ ← max. 1 value and its 2 coordinates of $\left|\right.$ gradient-based solving of Poisson equation($\boldsymbol{x}(i,j)$) - $\boldsymbol{x}(i,j)\left|\right.$

4: ***Feature vector***(9-D) ← $\mathcal{VG}$, $\mathcal{VF}$, $\mathcal{RRP}$

Machine Learning:

Train image:

1: ***Positive data*** ← ***Feature vector***(Median-filtered($\boldsymbol{x}$))

2: ***Negative data*** ← ***Feature vector***(Other type($\boldsymbol{x}$))

3: **SVM Classifier model** ← **SVM**(***Positive data***, ***Negative data***)

Test image:

1: ***Positive data*** ← ***Feature vector***(Median-filtered($\boldsymbol{x}$))

2: ***Negative data*** ← ***Feature vector***(Other type($\boldsymbol{x}$))

3: ***AUC***, $\boldsymbol{\delta}$, $\boldsymbol{P_e}$, and $\underline{\boldsymbol{P}_{\mathrm{TP}}@P_{\mathrm{FP}}=0.01}$ ← **SVM Classifier model**(***Positive data***, ***Negative data***)

Median filtering detection:

1: Decision of ***MFD*** ← $\boldsymbol{x}$(max(***AUC***)|max($\boldsymbol{\delta}$)|min($\boldsymbol{P_e}$)| max($\underline{\boldsymbol{P}_{\mathrm{TP}}@P_{\mathrm{FP}}=0.01}$))

4. Experiment and discussion

This section describes the experimental method for training the SVM classifier. The image databases for the training and testing are also constructed for several altered image types. The experimental results of the proposed variation- and residual-based MF detectors were compared with those of the MFR AR [3] and MFF OBC [1] schemes, respectively, for the verification of the effectiveness.

The MFR AR has a 10-D feature vector that shows good performance, and the performance of the 9-D MFF OBC feature vector outperforms the other subsets of the MFF regarding the classification ratio. The MFR AR and MFF OBC exhibit excellent performance among the existing MF detectors. Therefore, the proposed scheme is comparable to the schemes in [1,3].

The experiments were conducted using MATLAB (R2016a) tools in a PC environment (64-bit version of Windows 7, Intel core i7-5960X CPU @ 3.00 GHz and DDR4 32 GB memory).

4.1. Experimental method

It uses the constructed 9-D feature vector of the proposed scheme as input for the SVM classifier for MF detection training. A C-SVM with a Gaussian kernel [12] is employed as the classifier:

$$K\left(x_i, x_j\right) = \exp\left(-\gamma \parallel x_i - x_j \parallel^2\right) (\gamma > 0). \tag{20}$$

The proposed feature vector was trained in the SVM classifier with five-fold cross-validation in conjunction with a grid search to obtain the best parameters of c and γ in the multiplicative grid:

$$(C,\gamma) \in \{(2^i 2^j) | 4\times i, 4\times j \in Z. \tag{21}$$

The searching step size of (i, j) is 0.2; these parameters are then used to obtain the classifier model on the training set.

4.2. Image database and training–testing pairs

In experiments, the composite image database COMP was constructed using the three following image databases:

1. The COMP$_{BOWS2}$ image database (http://bows2.ec-lille.fr/), which consists of 10,000 downsampled and cropped natural grayscale images of fixed size 512 $\times$ 512.
2. The COMP$_{UCID}$ image database [13], which consists of 1338 uncompressed color images of size 512 $\times$ 384 or 384 $\times$ 512; where necessary, the images were converted to 8-bit grayscale images.
3. The COMP$_{SAM}$ image database (http://www.shsu.edu/$\sim$qxl005/New/Downloads/index.html), which is a raw image database containing 5150 uncompressed raw color images of size 256 $\times$ 256; where necessary, the images were also converted to 8-bit grayscale images.

In training and testing the 16,488 images, COMP$_{ALL}$ is prepared for unaltered (ORI), 3 $\times$ 3 median filtering (MF3), 5 $\times$ 5 median filtering (MF5), 3$\times$3 averaging filtering (AVE3), QF = 90 JPEG (JPG90), QF = 70 JPEG (JPG70), 3 $\times$3 Gaussian filtering (GAU3), 90% downscaling (DN0.9), and 110% upscaling (UP1.1). A total of 10,000 images randomly selected for the training will be used: 6000 images from the BOWS2 database, 900 images from the UCID database, and 3100 images from the SAM database. The remaining 6488 images will be used for testing.

For the implementation of the SVM classifier model, the MF3, MF5, and MF35 (composed of 5000 MF3 and MF5 images randomly selected) images are prepared for positive data in SVM classifier training for MF detection. The negative data also consist of the three groups: A, B, and C, as shown in Table 1.

Table 1. Groups A , B, and C of the negative data for SVM training.

Group A: the unaltered images and the images altered just once	**Group B:** post-altered two times more after MF3 and pre- and post-altered after MF3	**Group C:** post-altered two times more after MF5 and pre and post-altered after MF5
•ORI	•MF3 + AVE3 + JPG70	•MF5 + AVE3 + JPG70
•AVE3	•MF3 + GAU3 + JPG70	•MF5 + GAU3 + JPG70
•JPG90	•MF3 + DN0.9 + JPG70	•MF5 + DN0.9 + JPG70
•JPG70	•MF3 + UP1.1 + JPG70	•MF5 + UP1.1 + JPG70
•GAU3	•JPG90 + MF3 + JPG70	•JPG90 + MF5 + JPG70
•DN0.9	•JPG70 + MF3 + JPG70	•JPG70 + MF5 + JPG70

4.3. Experimental results

For the effective measurement of the proposed scheme in the experiment, the four measured experimental items are the following: the area under the ROC curve (AUC), the classification ratio, the minimal average decision error (Pe), and $P_{TP}@P_{FP} = 0.01$ (P_{TP} and P_{FP} denote the true positive and false positive rates, respectively).

$$P_e = min(\frac{P_{FP} + 1 - P_{TP}}{2}). \tag{22}$$

The trained SVM classifier model is subsequently used to perform MF detection, and the measurement procedure is repeated 30 times to reduce the variations in performance caused by the different selections of training samples. Detection accuracy, which is the arithmetic average of the true positive rate (TP) and the true negative rate (TN), is averaged 30 times through random experiments, which is similar to [6].

The average processing time for feature extraction and SVM training/testing is summarized in Table 2. The computing process of the MFR AR scheme gets the power spectral density based on an autoregressive model in statistics and signal processing. The computing process of the MFF OBC gets an occurrence of the block-center gray level by only searching and sorting algorithms in the spatial domain. The proposed scheme gets one-third features in the spatial domain and two-third features in the spectral domain, respectively.

Table 2. The average processing time for feature extraction and SVM training/testing.

MFD scheme	MFR AR 10-D [3]	MFF OBC 9-D [1]	Proposed scheme 9-D
Computing algorithm	Autoregressive model in statistics and signal processing	Block-center gray level by searching and sorting	Signal processing
Feature extraction	0.4847 s	0.6908 s	0.1422 s
SVM training	7.2846 s	6.3616 s.	6.3425 s

Feature extraction time: averaged 30 times when the image size is 512 × 512 of the gray scale.
SVM training time: averaged 30 times when the positive and negative data are 330, respectively, for 12 image types selected randomly from groups A, B, and C.

In Table 2, it can be observed that with the computing algorithm using the MATLAB toolbox, the signal processing method is faster. The feature metrics of the MFR AR, MFF OBC, and the proposed scheme for nine image formats are distributed in Figure 4. In these, the y-axis plots the feature vector values of the sample images in all image formats, which is similarly depicted in [5,14,15].

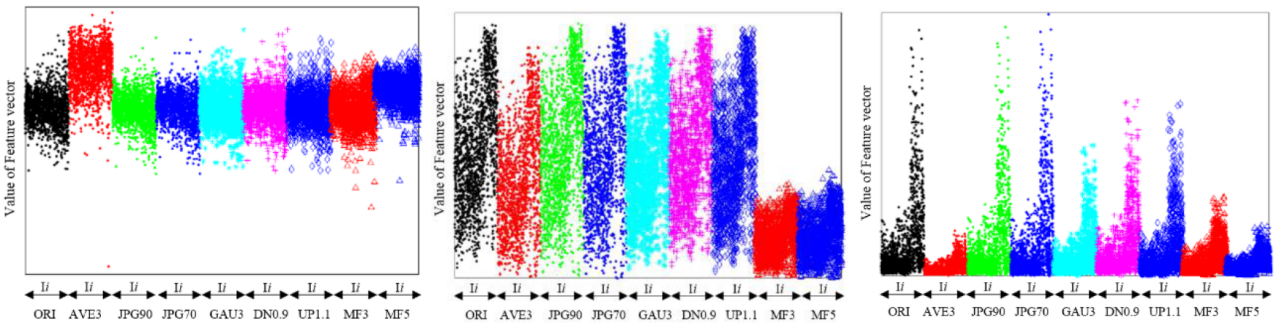

Figure 4. Feature set distributions (Ii: Image index 1–16,488): a) MFR AR 10-D [3]; b) MFF OBC [1]; c) proposed scheme from different types of sample images of group A: original, average filtering ($w = 3 \times 3$); JPEG compression (QF = 90); JPEG compression (QF = 70); Gaussian filtering ($w = 3 \times 3$ and $\sigma = 0.5$); downscaling (size = 0.9); upscaling (size = 1.1); median filtering ($w = 3 \times 3$); median filtering ($w = 5 \times 5$), where w: window size.

First, MFF OBC [1], MFR AR [3], and the proposed scheme are executed in the prepared experimental environment under the same conditions. In Figures 5, 6, and 7, the ROC curves show the performance of MF w where ($w \in \{3, 5, 35\}$) versus the test images (full size) of groups A, B, and C of the results of MFR AR, MFF OBC, and the proposed scheme, respectively.

In Figure 5, the MFR AR scheme performs the best in groups B and C, which are post- or pre-altered twice more after MF3 and MF5. In this part, the ROC curves of the detector show a higher P_{TP} for all P_{FP} rates. In group A, the performance of detecting MF in GUS3, ORI, DN0.9, and JPG90 was low, and the performance of detecting MF in AVE3, UP1.1, and JPG90 was good.

In Figure 6, the MFF OBC scheme performs best in MF3 versus the test images of groups B and C, which are post- or pre-altered twice more after MF3 and MF5. In this part, the ROC curves of the detector show a higher P_{TP} for all P_{FP} rates. In group A, the performances of MF detection in AVE3 and JPG70 are lower and higher, respectively. For the rest of the image types, the performances are good.

From now on, the proposed scheme occurs in the same manner as the MFR AR and MFF OBC examined before. In Figure 7, the scheme exhibits excellent performance in MF3 versus all test images of groups A and B. In this part, the ROC curves of the detector show a higher P_{TP} for all P_{FP} rates of groups A and B. In MF35 versus the test images of group A, ORI is a bit low. Otherwise, the remaining types of images are excellent in groups A and B. Meanwhile, the performance of group C is lower than that of groups A and B. In group C, MF3 versus 'MF5 + UP1.1 + JPG70' is low, and the rest of the image types are slightly better. Subsequently, the detection of MF in many test image types in groups A, B, and C allowed for performance evaluation and theoretical analysis. The experimental results of the test images on AUC with respect to sensitivity (P_{TP}: true positive rate) and 1 – specificity (P_{FP}: false negative rate), classification ratio, P_e, and $P_{TP}@P_{FP} = 0.01$ in low-resolution 32×32, 64×64 block size and the full-size images, respectively, are shown in Table 3. The results of four experimental items dealing with the testing for each group and MF w are averaged. In this evaluation for each training–testing pair, the term of general interpretation AUC is used.

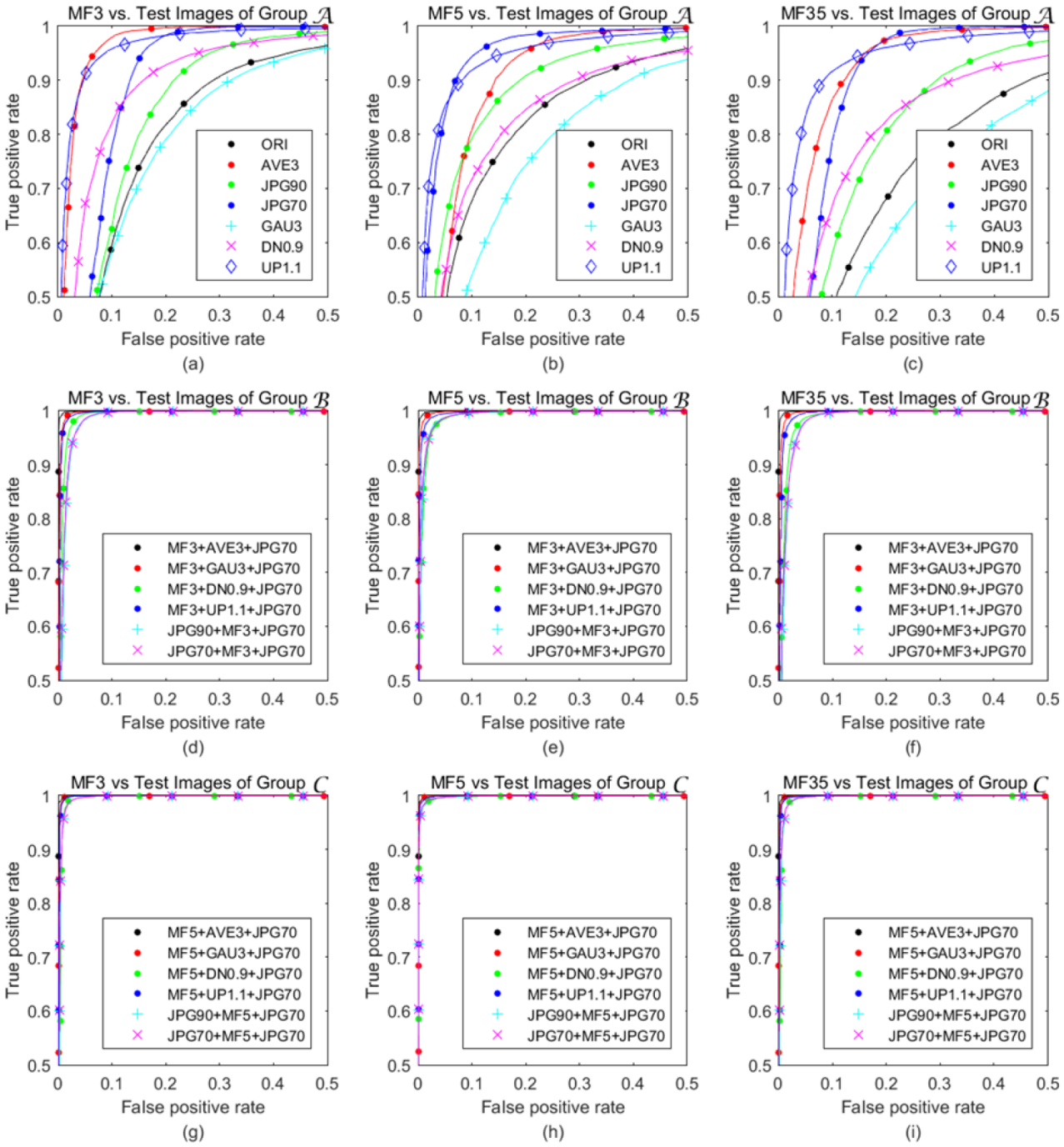

Figure 5. ROC curves: MF3 (a, d, and g), MF5 (b, e, and h), and MF35 (c, f, and i) detection performance on groups A, B, and C of MFR AR [3].

First, MFF OBC [1], MFR AR [3], and the proposed scheme are executed in the prepared experimental environment under the same conditions. In Table 3, the performance of MFw (where $w \in \{3, 5, 35\}$) versus the test images of groups A, B, and C are shown, and the experimental results of MFR AR, MFF OBC, and the proposed scheme are compared.

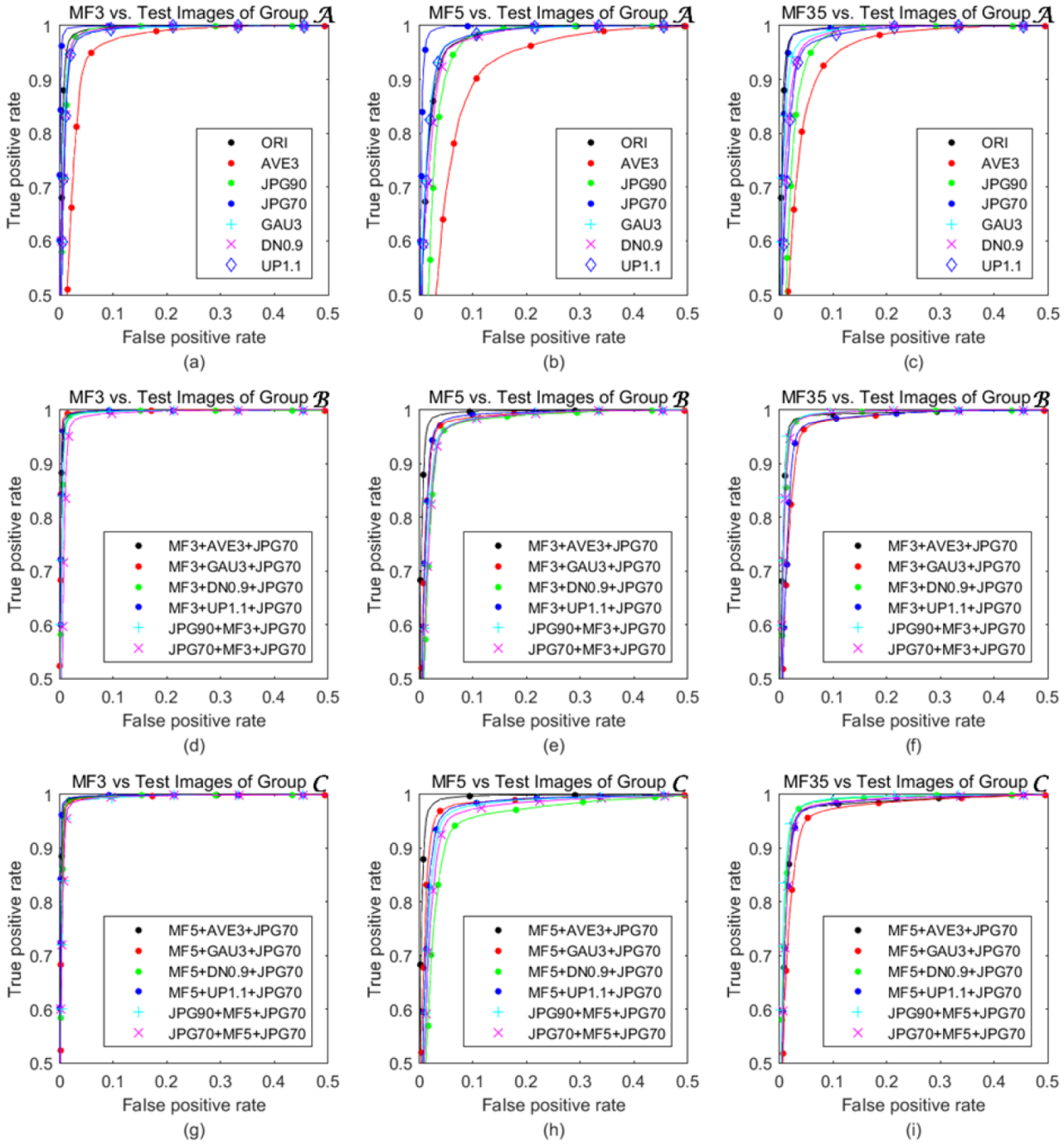

Figure 6. ROC curves: MF3 (a, d, and g), MF5 (b, e, and h), and MF35 (c, f, and i) detection performance on groups A, B, and C of MFF OBC [1].

From Table 3, the MFR AR scheme performs the best on the partly full-size test images of group C, which are post- or pre-altered twice more after MF3, MF5, and MF35. The MFF OBC scheme performs the best in MF3 versus the full-size test images of group B, which is post- or pre-altered twice more after MF3. The proposed scheme exhibits excellent performance of MF3, MF5, and MF35 on all test image sizes (32 $\times$ 32, 64 $\times$ 64, and full size) of groups A, B, and C, except the partly full-size test images from group C.

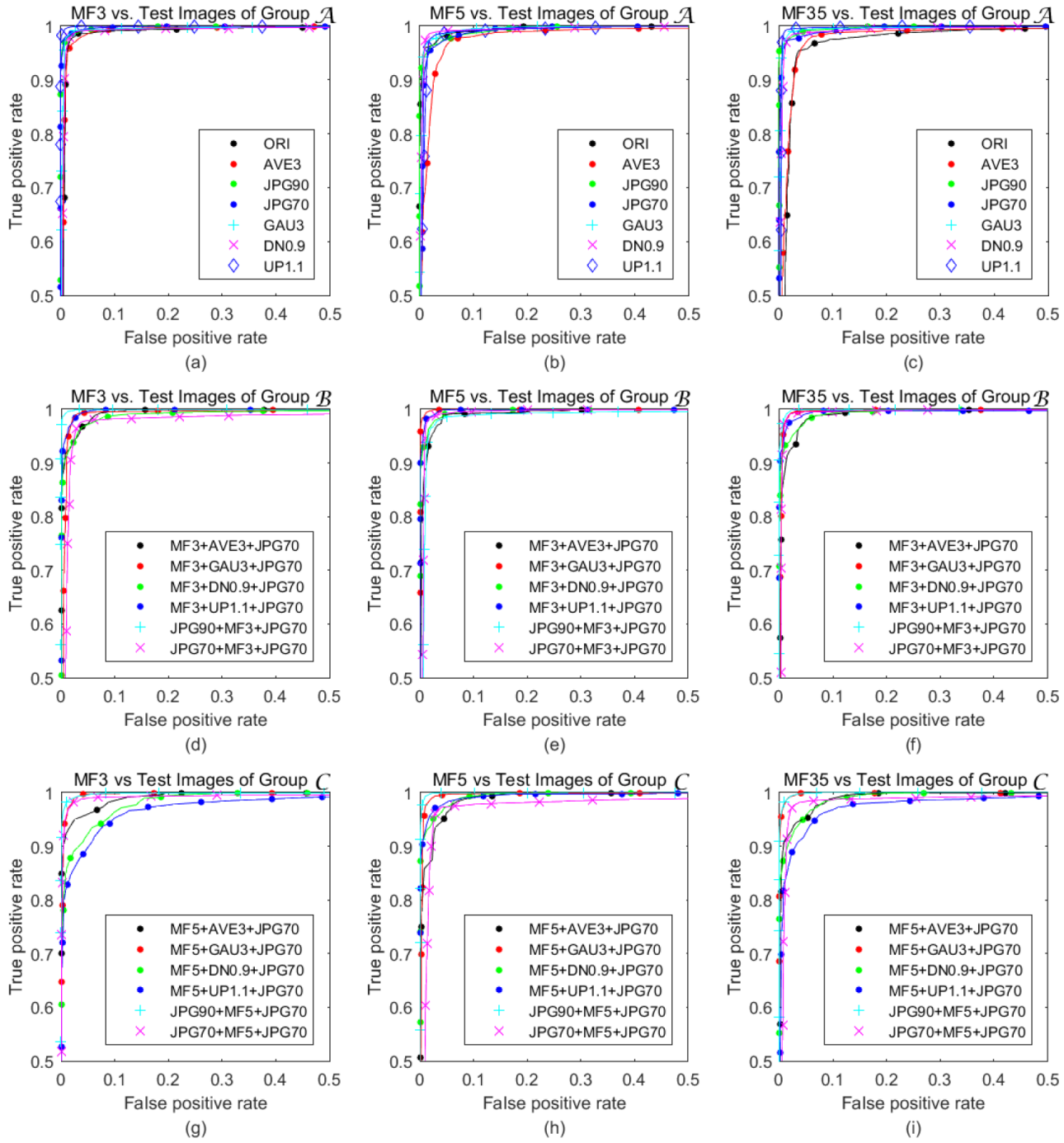

Figure 7. ROC curves: MF3 (a, d, and g), MF5 (b, e, and h), and MF35 (c, f, and i) detection performance on groups A, B, and C of the proposed variation- and residual-based median filtering detection scheme.

The classified rate of the experimental AUC results is interpreted using the traditional academic point system (http://gim.unmc.edu/dxtests/roc3.htm). Through the measured results of the four items in the 32 × 32 block size (a), 64 × 64 block size (b), and full size (c), the proposed scheme is rated as "*Excellent* (*A*)" according to the AUC, which is above 0.9. The dominant performance of the proposed scheme is quite apparent.

Table 3. Performance comparison between MFR AR, MFF OBC, and the proposed scheme on block size a) 32 × 32, b) 64 × 64, and c) full-sized images, respectively.

MF detection schemes	MFw	No.	(a) 32 × 32 block size image			(b) 64 × 64 block size image			(c) Full-size image		
			Test images of group			Test images of group			Test images of group		
			A	B	C	A	B	C	A	B	C
MFR AR 10-D [3]	MF3	1	0.9246	0.9418	0.9647	0.8826	0.8943	0.9090	0.9234	0.9950	**0.9978**
		2	0.7514	0.6467	0.6127	0.5941	0.4575	0.3857	0.2650	0.8625	0.9597
		3	0.0929	0.0827	0.0542	0.1531	0.1425	0.1240	0.1229	0.0175	0.0090
		4	0.8800	0.8872	0.9308	0.8684	0.8532	0.8540	0.8254	0.9610	0.9780
	MF5	1	0.9527	0.9533	0.9627	0.9274	0.9187	0.9238	0.9159	0.9963	**0.9993**
		2	0.8481	0.8103	0.7307	0.7369	0.6635	0.6005	0.2734	0.9173	**0.9883**
		3	0.0641	0.0660	0.0545	0.1080	0.1167	0.1063	0.1386	0.0177	0.0073
		4	0.9199	0.9087	0.9182	0.8966	0.9115	0.8848	0.8051	0.9673	0.9885
	MF35	1	0.9336	0.9497	0.9530	0.9041	0.9065	0.9182	0.8844	0.9942	**0.9982**
		2	0.7824	0.7608	0.5763	0.6709	0.6077	0.4665	0.1891	0.8463	0.9655
		3	0.0837	0.0703	0.0682	0.1304	0.1283	0.1133	0.1676	0.0198	0.0090
		4	0.9019	0.8880	0.9197	0.8874	0.8942	0.8788	0.7870	0.9585	0.9808
MFF OBC 9-D [1]	MF3	1	0.9389	0.9467	0.9317	0.9684	0.9780	0.9700	0.9917	**0.9967**	0.9968
		2	0.2766	0.2898	0.2503	0.4969	0.5988	0.5893	0.8426	0.9240	0.9350
		3	0.1047	0.0967	0.1218	0.0629	0.0503	0.0652	0.0230	0.0115	0.0117
		4	0.7724	0.7947	0.7585	0.8266	0.8617	0.8310	0.8880	0.9403	0.9340
	MF5	1	0.9186	0.9103	0.8798	0.9466	0.9450	0.9222	0.9809	0.9885	0.9850
		2	0.2036	0.1637	0.1395	0.3110	0.2813	0.2732	0.6837	0.7998	0.7970
		3	0.1260	0.1370	0.1755	0.0857	0.0940	0.1258	0.0449	0.0302	0.0377
		4	0.7474	0.7370	0.6860	0.7940	0.7920	0.7465	0.8654	0.9037	0.8913
	MF35	1	0.9264	0.9265	0.9068	0.9547	0.9588	0.9472	0.9864	0.9912	0.9885
		2	0.2290	0.2142	0.1970	0.3844	0.4042	0.4182	0.7497	0.8525	0.8375
		3	0.1176	0.1213	0.1507	0.0806	0.0813	0.1012	0.0367	0.0253	0.0320
		4	0.7571	0.7622	0.7247	0.8043	0.8160	0.7908	0.8794	0.9127	0.8932
Proposed scheme 9-D	MF3	1	**0.9924**	**0.9942**	**0.9883**	**0.9941**	**0.9882**	**0.9882**	**0.9963**	0.9943	0.9955
		2	**0.9371**	**0.9617**	**0.9532**	**0.9600**	**0.9567**	**0.9567**	**0.9753**	**0.9708**	**0.9722**
		3	**0.0116**	**0.0093**	**0.0177**	**0.0081**	**0.0175**	**0.0175**	**0.0054**	**0.0077**	**0.0080**
		4	**0.9874**	**0.9910**	**0.9755**	**0.9901**	**0.9825**	**0.9825**	**0.9924**	**0.9878**	**0.9892**
	MF5	1	**0.9840**	**0.9917**	**0.9917**	**0.9887**	**0.9947**	**0.9947**	**0.9944**	**0.9967**	0.9947
		2	**0.8787**	**0.9210**	**0.9447**	**0.9169**	**0.9728**	**0.9728**	**0.9599**	**0.9805**	0.9735
		3	**0.0221**	**0.0130**	**0.0138**	**0.0169**	**0.0088**	**0.0088**	**0.0096**	**0.0052**	**0.0070**
		4	**0.9670**	**0.9835**	**0.9852**	**0.9759**	**0.9908**	**0.9908**	**0.9883**	**0.9940**	**0.9888**
	MF35	1	**0.9867**	**0.9945**	**0.9913**	**0.9941**	**0.9947**	**0.9947**	**0.9927**	**0.9973**	0.9948
		2	**0.8996**	**0.9520**	**0.9513**	**0.9446**	**0.9752**	**0.9752**	**0.9496**	**0.9713**	**0.9725**
		3	**0.0183**	**0.0087**	**0.0138**	**0.0093**	**0.0087**	**0.0087**	**0.0109**	**0.0047**	**0.0072**
		4	**0.9743**	**0.9907**	**0.9810**	**0.9880**	**0.9892**	**0.9892**	**0.9851**	**0.9942**	**0.9923**

Best results for each training–testing pair are displayed in bold.
MFw: Median filtering window size, $w \in \{3, 5, 35\}$.
No. (experimental result item) 1: AUC; 2: $P_{TP}@P_{FP} = 0.01$; 3: P_e; 4: classification ratio.

An example of a cut-and-paste forgery image is shown in Figure 8. An unaltered image (arch gate) is cut, and a median-filtered image (house) is pasted onto the cut area (empty region) of the unaltered image (those unaltered images come from the BOWS2 database), forming a composite image, which is then JPEG post-compressed using a quality factor of 90 or rotated counterclockwise by 5°. The forming of the cut-and-paste is similar to [16]. The MF detection blocks with (a) the MFR AR, (b) the MFF OBC, and (c) the proposed scheme are shown in Figure 9. The detected median-filtered blocks (the true alarms) appear in red, and the remaining blocks (the false alarms) appear in blue. In each of the schemes in Figure 9, the left column (a, c, and e) is examined in a 32 × 32 block size, and the right column (b, d, and f) is examined in a 64 × 64 block size. The first row (a and b) shows the detection results in MF3 versus the unaltered images, the second row (c and d) shows the detection results in MF3 + JPG90 versus the JPEG90 images, and the last row (e and

f) shows the detection results in MF3 versus the unaltered to rotated images. The proposed scheme efficiently detects the median-filtered images in Figure 9.

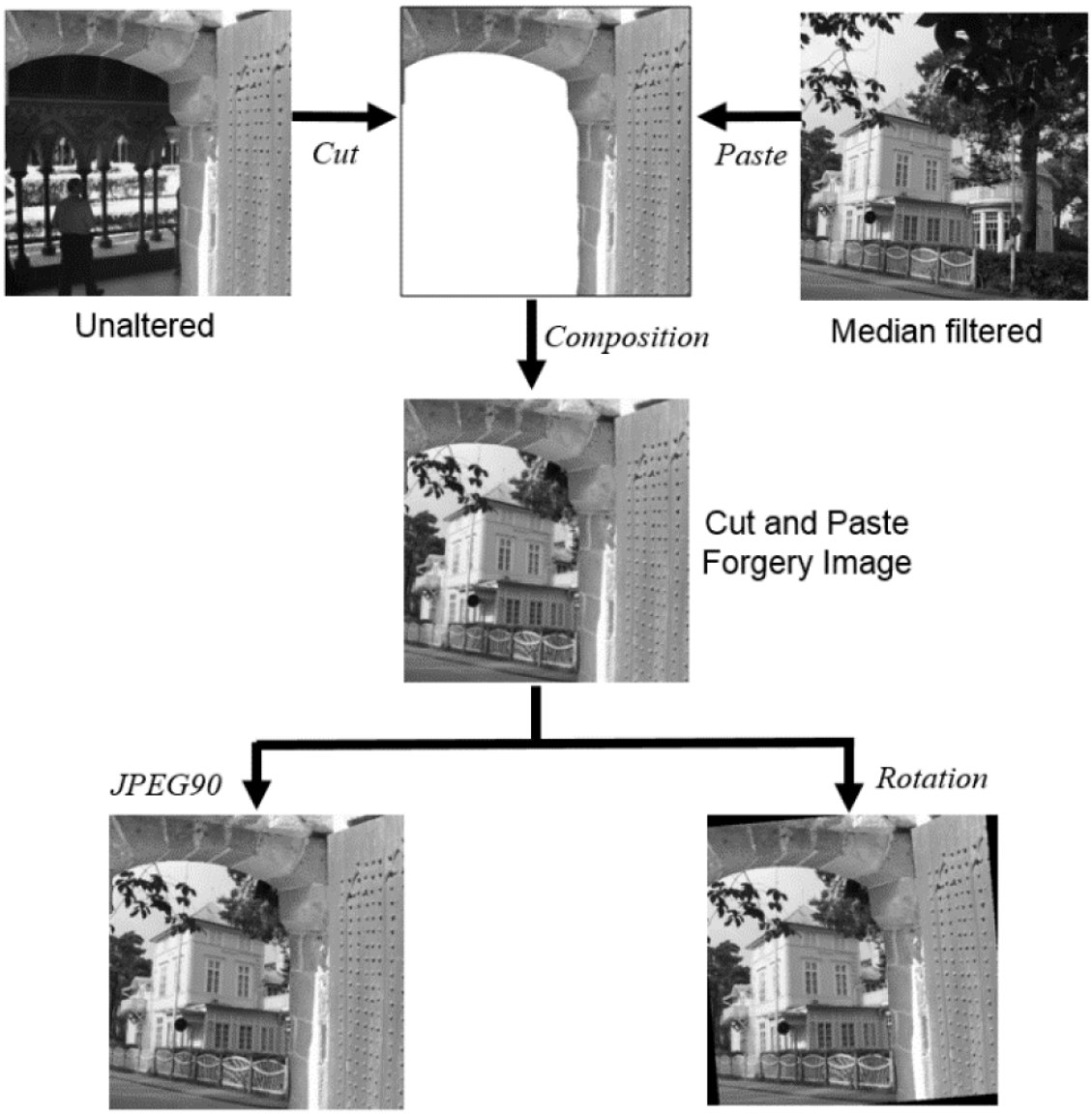

Figure 8. A cut-and-paste forgery image example.

5. Conclusion

In this paper, a new variation- and residual-based MF detection scheme is proposed. The 9-D feature vector length is constructed in a similar way as the 9-D MFF OBC or shorter than the 10-D MFR AR. Three feature sets in the feature vector are extracted from the spatial and spectral domain, and the residual image by the gradient-based solving of Poisson's equation. However, it aims to achieve a higher classification ratio with a short feature vector length for MF detection.

Nevertheless, the performance evaluation results are useful. The AUC, classification ratio, and $P_{TP}@P_{FP} = 0.01$ are achieved to 1, and P_e is achieved to 0. In particular, MF detection in JPEG post-compression is supreme.

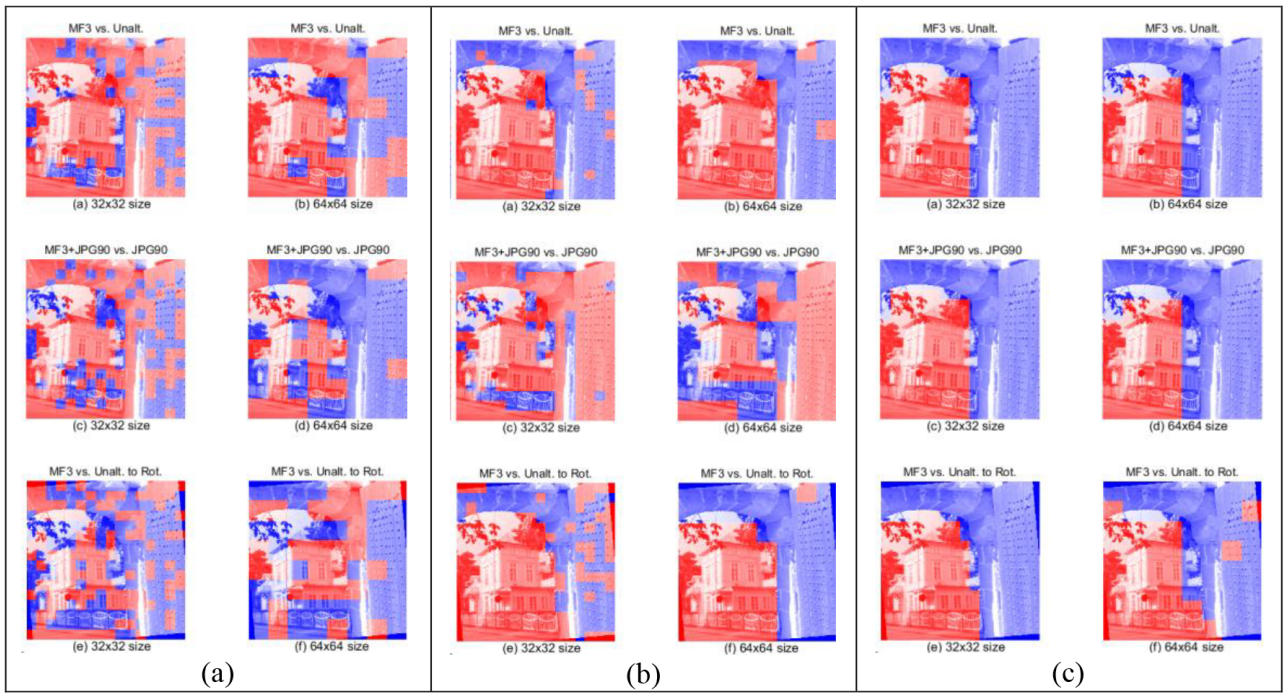

Figure 9. Local median filtering detection results: a) MFR AR 10-D [3], b) MFF OBC scheme [1], and c) the proposed scheme.

To the best of our knowledge, this approach is a complete solution that considers both the gradient aspects and the residual in the image. Therefore, these results serve to further MF detection research.

In the future, the proposed scheme can be expected to solve MF detection of forensic problems.

Acknowledgment

This research study was supported by the Ministry of Trade, Industry, and Energy (MOTIE), Korea, through the Education Support Program for Creative and Industrial Convergence (Grant Number N0000717).

References

[1] Yuan H. Blind forensics of median filtering in digital images. IEEE T Inf Foren Sec 2011; 6-4: 1335-1345.

[2] Kang Hyeon RHEE. Median filtering detection using variation of adjacent line pairs for image forensic. In: IEEE 5th International Conference on Consumer Electronics; 2015; Berlin, Germany. pp. 103-107.

[3] Kang X, Stamm MC, Peng A, Liu KJR. Robust median filtering forensics using an autoregressive model. IEEE T Inf Foren Sec 2013; 8: 1456-1468.

[4] Chen C, Ni J, Huang J. Blind detection of median filtering in digital images: a difference domain based approach. IEEE T Image Process 2013; 22: 4699-4710.

[5] Kirchner M, Fridrich J. On detection of median filtering in digital images. SPIE Media Forensics and Security 2010; 2: 1-12.

[6] Zhang Y, Li S, Wang S, Shi YQ. Revealing the traces of median filtering using high-order local ternary patterns. IEEE Signal Proc Let 2014; 21: 275-280.

[7] Gui X, Li X, Qi W, Yang B. Blind median filtering detection based on histogram features. In: Annual Summit of the Asia-Pacific Signal and Information Processing Association; 9–12 December 2014; Siem Reap, Cambodia. pp. 1-4.

[8] Ke Y, Qin F, Min W, Zhang Q. An efficient blind detection algorithm of median filtered image. International Journal of Hybrid Information Technology 2015; 8: 181-192.

[9] Kay SM. Modern Spectral Estimation: Theory and Application. Englewood Cliffs, NJ, USA: Prentice Hall, 1998.

[10] Fattal R, Lischinski D, Werman M. Gradient domain high dynamic range compression. ACM T Graphic 2002; 21: 249-256.

[11] Raskar R, Tan KH, Feris R, Yu J, Turk M. Non-Photorealistic Camera: Depth Edge Detection and Stylized Rendering Using Multi-Flash Imaging. Mitsubishi TR2006-107. Tokyo, Japan: Mitsubishi, 2006.

[12] Chang CC, Lin CJ. LIBSVM: a library for support vector machines. ACM Transactions on Intelligent Systems and Technology 2011; 2: 1-27.

[13] Schaefer G, Stich M. UCID-an uncompressed color image database. In: Proceedings of Storage and Retrieval Methods and Applications for Multimedia Conference; 18 January 2004; San Jose, CA, USA. Bellingham, WA, USA: SPIE. pp. 472-480.

[14] Cao G , Zhao Y , Ni R , Yu L, Tian H. Forensic detection of median filtering in digital images. In: IEEE International Conference on Multimedia and Expo; 19–23 July 2010; Singapore. pp. 89-94.

[15] Xu J, Ling Y, Zheng X. Forensic detection of Gaussian low-pass filtering in digital images. In: 8th International Conference on Signal and Image Processing; 14–16 October 2015; Shenyang, China. pp. 819-823.

[16] Kang Hyeon RHEE. Median filtering detection using variation of neighboring line pairs for image forensics. Journal of Electronic Imaging 2016; 25: 1-13.